International Journal of Heat and Mass Transfer 52 (2009) 355–365

Contents lists available at ScienceDirect

International Journal of Heat and Mass Transfer

journal homepage: www.elsevier.com/locate/ijhmt

An experimental study of natural convection in a differentially heated cavity through a 2D-PIV system

F. Corvaro *, M. Paroncini

Dipartimento di Energetica, Università Politecnica delle Marche, Via Brecce Bianche, 60100 Ancona, Italy

ARTICLE INFO

Article history:
Received 30 July 2007
Received in revised form 20 May 2008
Available online 15 August 2008

Keywords:
Natural convection
2-D PIV
Differentially heated cavity

ABSTRACT

This paper provides an experimental analysis of the natural convection in a differentially heated H side square enclosure. The cavity is full of air and is heated by a hot strip with a height of $H/2$. The effect of the position of this source on the dynamic structures generated by the natural convection heat transfer was analyzed at the steady state and under laminar conditions. The experimental apparatus is a 2D-PIV system while the experimental data consist of vector maps, velocity maps and streamlines at different Rayleigh numbers. During the study the presence of two small vortexes was noted on the upper surface of the source. These are dependent both on the Rayleigh numbers and on the position of the strip.

1. Introduction

The study of natural convection heat transfer is important because it is used in many engineering applications. Natural convection is cheap and is not dependent on any type of electromechanical equipment. For these reasons it is used, for example, in solar energy systems, in the cooling of electronic circuits, in air conditioning and in many other fields, and is therefore very important for applied research.

Technical literature offers numerous studies of natural convection in a square cavity and many of these studies analyze the convective phenomenon through numerical simulations. However, very few works show experimental data about this physical phenomenon using a 2D-PIV system.

Cesini et al. [1] analyzed the convective heat transfer generated by a horizontal cylinder located in a square cavity. This study was carried out both through an experimental analysis and through a numerical study. Ramos and Milanez's [2] paper deals with natural convection in cavities heated from below through a thermal source, which dissipated energy at a constant rate. Valencia and Frederick [3] elaborated a numerical investigation on the heat transfer of air in square cavities with partially active vertical walls. Aydin and Yang [4] simulated numerically the natural convective heat transfer in air in a square cavity cooled by the side walls and heated by a strip placed at the centre of the bottom wall. Ntibarufata et al. [5] analyzed numerically natural convection in partitioned enclosures with localized heating from below. Oztop and Bilgen [6] made a numerical study on natural convection in differentially heated and partially divided square cavities with internal heat generation. Their results acted as an interesting starting point for the experimental analysis in this paper. Stickland et al. [7] also carried out an experimental investigation of natural convection in a differentially heated cavity with solidification of water.

Acharya and Jetli [8] studied numerically natural convection in a partially divided square box where the lateral walls were at different temperatures and the single partial divider was not heated. Finally, Anderson and Bejan [9] analyzed natural convection through single and double vertical walls but even in this case the different dividers were not heated.

In this paper, the natural convection generated by a hot divider source of height h in a square enclosure is analyzed. Air ($Pr = 0.71$) was used as fluid in the cavity. The choice of air makes this work interesting because it is not easy to find experimental results for this fluid in natural convection using a PIV system. This is probably due to the difficulties that are encountered when developing an experimental set-up which produces acceptable data.

The testing cavity was a square enclosure (height $H = 0.05$ m) and the influence of the position of a heated strip (width $l = 0.01$ m and height $h = H/2$) on the natural convection heat transfer was analyzed. The heated strip was placed on the bottom of the cavity which was cooled through all the lateral walls at the same time.

Three different positions of the hot strip were analyzed: $d = 0.02$ m (the central position), $d = 0.015$ m and $d = 0.01$ m from the right lateral wall.

The dynamic structures, generated by the natural convection heat transfer, were analyzed using 2D Particle Image Velocimetry. With this experimental equipment the distributions of the velocity vectors, the streamlines and the velocity fields at different Rayleigh

* Corresponding author. Tel.: +39 071 2204276; fax: +39 071 2204770.
E-mail address: f.corvaro@univpm.it (F. Corvaro).

0017-9310/$ - see front matter © 2008 Elsevier Ltd. All rights reserved.
doi:10.1016/j.ijheatmasstransfer.2008.05.039

Nomenclature

g	modulus of the gravity vector ($g = 9.81$ m s^{-2})
Δt	time between two laser pulses (μs)
H	square cavity side (m)
k	thermal conductivity (W m^{-1} K^{-1})
l	heat source length (m)
d	position of the heat source with respect to the right lateral cold wall (m)
L	cavity depth of the experimental test sections (m)
Pr	Prantdl number
Ra	Rayleigh number
T	temperature (K)
T_m	average temperature (K)
$\Delta T = (T_h - T_c)$	temperature difference between heat source and cold plates (K)
x,y	Cartesian coordinates

Greek symbols

β	thermal expansion coefficient (K^{-1})
ν	kinematic viscosity (m^2 s^{-1})
ρ	density (kg m^{-3})

Subscripts

c	cold wall
h	hot wall

numbers were obtained. In particular, the aim was to evaluate the influence of the position of the hot strip on the vortexes created by the air flow due to the thermal rate.

The experimental research analyzed different Rayleigh numbers, in particular from 6.5×10^4 to 3.2×10^5. Moreover, the quality of the experimental data in each test was also evaluated to assess the repeatability of the tests and the stationary state of the physical phenomenon.

2. Experimental set-up

The main components of the experimental system, shown in Fig. 1, include the test cell, filled with air at atmospheric pressure, the 2D-PIV system, two thermostatic baths and the data acquisition system. Fig. 2 shows a sketch of the experimental set-up.

The test cell, shown in Fig. 3, had a square section of $H = 0.05$ m. The heat source, made of aluminium to allow for good thermal conductivity, was positioned on the lower horizontal wall with a temperature T_h, that was maintained constant through the continuous circulation of a thermostatic fluid. This temperature was changed from one test to another in order to obtain, different Rayleigh numbers for each test. The heat source had a height of $h = 0.025$ m and width $l = 0.01$ m. The length of the source was the same as that of the test cavity.

The lateral vertical walls, that were also made of aluminium, were cooled at a uniform temperature T_c by a different fluid which was itself cooled by another thermostatic bath. This temperature was set at 291.16 K and was maintained constant during each test.

Fig. 1. The experimental set-up.

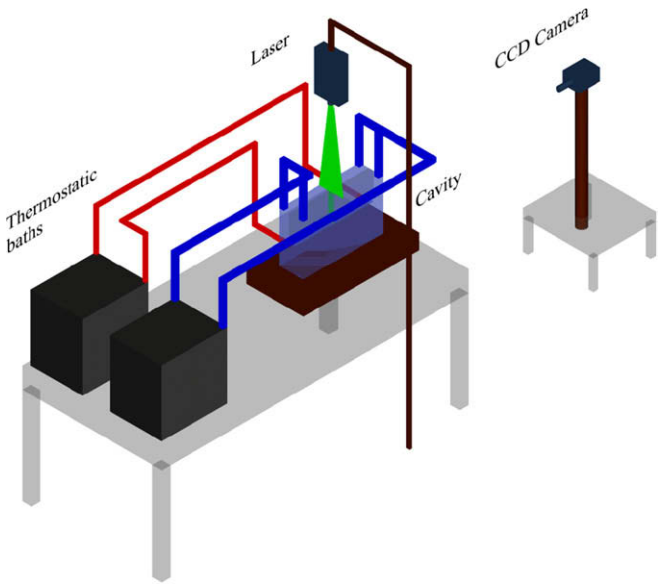

Fig. 2. Sketch of the experimental set-up.

The thermostatic circuit was made up of two thermostats with their respective connecting pipes. The thermostats were manufactured by the Lauda Company; the main characteristics of the PROLINE RP1840 model are shown in Table 1. Each pipe, which connected the thermostats with the inlet and outlet valves of the two sidewalls and the heater, was covered with a neoprene skin (about 0.02 m thick) to isolate it from heat loss. The thermostatic fluid was a mixture of 75% water and 25% glycol.

The front vertical wall was made of glass allowing optical access for the CCD camera. The top and the bottom surfaces of the enclosure were made of plexiglas so as to reduce to a minimum the heat leakage through these walls. In particular the upper plexiglas surface had a small opening at the rear end to allow the seeding to be inserted while the rear side was rigged with a 0.05 m square piece of wood to keep the seeding inside the cavity.

The test cell dimension in the longitudinal direction was $L = 0.41$ m; it was greater than H in order to ensure that it was long enough to limit the air motion developed along the z-axis, that was perpendicular to the laser beam, to such an extent that it became negligible. Consequently, the end effect could be neglected and the problem could be considered as a two-dimensional one.

The temperature of the test cell components was measured by 14 copper–constantan thermocouples. Ten thermocouples were located on the surfaces of the cool lateral walls with four of them on the surfaces of the heat source. These important parameters

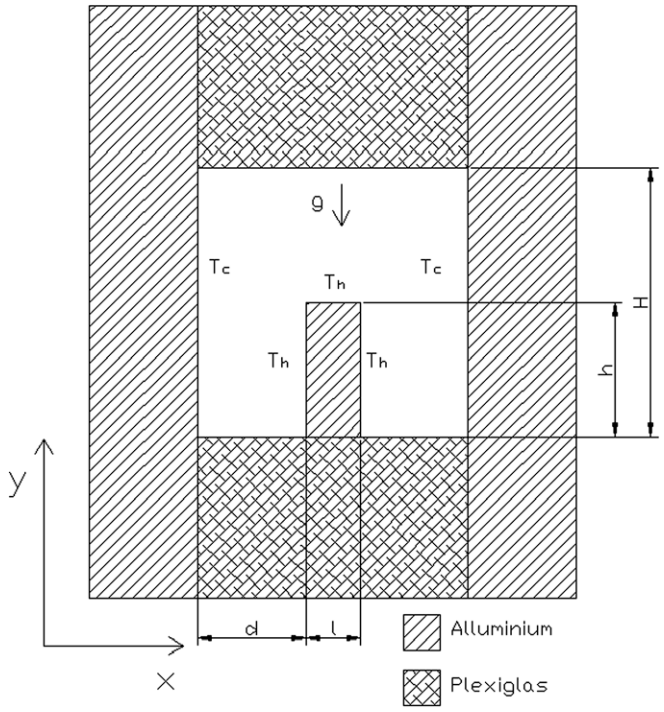

Fig. 3. The test cell.

Table 1
Main characteristics of thermostat

Operating temperature range (°C)	−40/200
Temperature accuracy (±°C)	0.01
Bath volume (l)	18
Class to EMC standard	B according to EN61326-1

were captured every 30 s during the experimental test through an acquisition system made up of a computer, that stored the measurements, and a data acquisition/switch unit, model Hp Agilent 34970A, that read in the temperature values. Each thermocouple was connected with an ice point reference made by Kaye, model K170. There was a maximum difference of 0.4 K between the stored temperatures recorded on the two lateral walls. Since the maximum temperature recorded on the cold wall was 291.86 K while the minimum was 291.46 K it was possible to consider that they had the same temperature. On the hot source the maximum and minimum temperatures captured were different according to the Rayleigh number analyzed although with a maximum difference of 0.3 K. Therefore, these surfaces can be considered isothermal.

Particle image velocimetry (PIV) is designed to make instantaneous velocity measurements in a cross-section of a flow. The PIV system provides the velocity fields by calculating the distance covered by the particles of the seeding when mixed with the air. In particular these particles have to be illuminated in one plane of the flow at least twice within a short time interval (Δt). The light scattered by the particles has to be recorded on two different frames. The displacement of the particle images between the light pulses is determined through evaluation of the PIV recordings.

The nature of the seeding particles must be chosen in order to provide a real description of the flow. For a more detailed explanation of the PIV technique, see Raffel et al. [10].

In our experiments oil particles were used and were nebulised by an air compressor system; the diameter of the particles was about 1 μm.

For these studies a 12 bit Hi Sense MkII Hamamatsu Camera C8484-05C with 1344 × 1024 pixels CCD camera was used to capture the images. The camera had a 60 mm Nikon lens which was covered by a filter with a wavelength of λ = 532 nm in order to record only the direct or scattered light from the laser source inside the PIV cavity.

A double cavity Nd-YAG laser with 30 mJ of energy, model Solo-II-15 with a wavelength of 532 nm, was used as a light source. The laser beam had variable pulse frequencies going from 1 to 15 Hz with a 10 ns duration of the pulsed illumination. For these experiments the laser was run at 5 Hz. The laser was also equipped with a lens system, producing a diverging light sheet not exceeding a 0.001 m thickness, and its own distilled water cooling system.

Data analysis of the PIV was performed using the software package "Dynamic Studio", described in detail in Dantec Dynamics [11].

The PIV recordings were analyzed using a Dell Precision PWS690 Intel® Xeon® computer with 1 GB RAM and with 4 RAID disks for a total memory capacity of 1 TB.

2.1. Experimental procedure

The laboratory where the tests were made was air-conditioned. The room temperature and the humidity conditions could be decided and checked: for each test a room temperature of 297 K and a relative humidity of 50% were set.

Before starting each experiment the seal of the cavity was checked to avoid any leakage of the seeding.

After these preliminary controls the thermostatic baths, set at the correct temperatures, were turned on. At this stage the thermostatic circuits were closed. When the thermostatic fluids inside each bath reached the target temperature the valves were opened to permit circulation both in the lateral walls and in the internal source. At the same time the acquisition system was started in order to capture the trend in the temperatures on the lateral walls and on the hot strip. Through this system it was also possible to check when the cold and the hot surfaces reached the isothermal condition. Only at this time was the flow inside the cavity checked to determine whether it was at the steady state. Twenty seconds before starting image acquisition, the oil particles were sprinkled inside the cavity through the small hole at the rear end of the upper plexiglas surface.

This step was very important. The introduction of the seeding generated a perturbation in the motion of air inside the cavity and it was therefore necessary to make the measurements only when the perturbation had disappeared and the flow had again reached the steady state. This happened in a very short time (10–15 s after the sprinkling) showing a very high physical stability of the phenomenon studied in this particular configuration.

The other important step was the choice of the time between two different laser pulses. In these experiments, performed using the PIV technique, it was one of the most important parameters to set. In fact, if this parameter is not correct the time between two different frames is either too short or too long to allow the correct displacement of each particle to be recorded. Consequently, it is impossible to evaluate the velocity field of the flow analyzed. Tables 2–4 show different Δt depending both on the Rayleigh numbers and on the position of the hot strip. The connection between the Rayleigh number and the time between two different laser pulses was very important in order to receive the best possible signal to noise ratio for a specific geometrical configuration. However, since the velocity fields changed with the Rayleigh number it was necessary to adjust this time before each test. In particular Δt decreased according to the growth in the Rayleigh number because the velocity field accelerated with the increase in the Rayleigh number. Normally a preliminary test was made in order to identify the Δt that gave the best average

Table 2
Times between two different laser pulses for the symmetrical configuration

$d = 0.02$ m	
Ra	Δt (μs)
6.39×10^4	18,000
1.21×10^5	14,000
1.78×10^5	12,000
2.28×10^5	9000
2.73×10^5	7000
3.16×10^5	5500

Table 3
Times between two different laser pulses for $d = 0.015$ m

$d = 0.015$ m	
Ra	Δt (μs)
6.39×10^4	19,000
1.21×10^5	15,000
1.78×10^5	13,000
2.28×10^5	10,000
2.73×10^5	8000
3.16×10^5	6500

Table 4
Times between two different laser pulses for $d = 0.01$ m

$d = 0.01$ m	
Ra	Δt (μs)
6.39×10^4	20,000
1.21×10^5	16,000
1.78×10^5	14,000
2.28×10^5	11,000
2.73×10^5	9000
3.16×10^5	7500

signal to noise ratio. An average signal to noise ratio of between 5 and 6 was obtained in each test.

Finally, using the CCD camera, it was possible to acquire images which were sent to the computer for analysis. The synchronization between laser emission and the CCD was controlled by the Dynamic Studio software developed by Dantec Dynamic. The time between the two laser pulses, the acquisition frequency, and the number of image pairs were set for each test. The light sheet entered through the upper part of the enclosure made of plexiglas and lit up a cross-section of the cavity in the middle of the cell. The camera, which was located perpendicularly to the light sheet, captured the images, which were then sent to the computer to be processed.

3. Results and discussion

In this section, the results of the experimental tests are presented. In particular the data for each Rayleigh number analyzed and for each different configuration are shown.

3.1. PIV analysis

The images, analyzed with Dynamic Studio using the "adaptive cross-correlation algorithm", were 1344×1024 pixels with an interrogation area of 32×32 pixels. Before each image processing, the images were masked to eliminate from the analysis the area outside the experimental chamber and the area which was taken up by the source. This procedure is very important since these areas would produce null vectors. An example of the image analyzed is shown in Fig. 4.

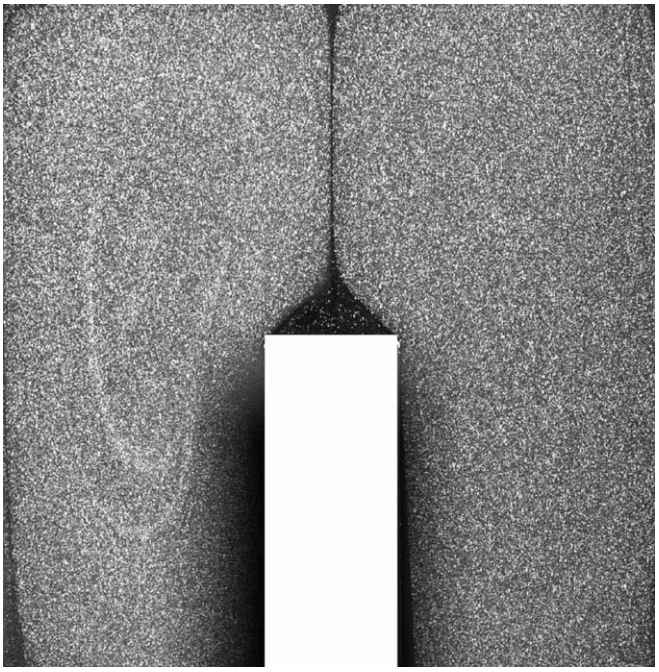

Fig. 4. A PIV image.

Adaptive cross-correlation is a non-intrusive method to measure the velocity vectors. An interrogation area of 32×32 pixels was used with three refinement steps, starting at 256×256 pixels. The overlaps in each interrogation area in the horizontal and vertical direction were 50%. Furthermore, a moving average validation was applied; this method validated vectors according to the comparison between neighbouring vectors: an averaging area of 3×3 number of refinements was used with an acceptance factor of 0.1 and 3 iterations. In each case the scope of post-processing was to identify any velocity vectors that were calculated wrongly. These errors may be connected with a lack of seeding particles in the interrogation area, the presence of high velocity gradients within the interrogation region, particles moving out of the interrogation region between successive images or the reflections of the cavity surfaces. When the wrong vector was identified it could be replaced by another one generated by the interpolation of the surrounding vectors using the method described. Further information about the algorithm used (adaptive cross-correlation) can be found in Dantec Dynamics [11] while Raffel et al. [10] give a detailed description of validation and replacement techniques.

In each test three data sets with 30 pairs of images were acquired for each Rayleigh number analyzed. Repeated PIV measurements allowed us to decide that 90 double frame pixel PIV images were sufficient in order to accurately and repeatedly determine the dynamic behaviour of the flow inside the cavity.

3.2. Repeatability

The repeatability of the experiment was also evaluated for each test. The same test was repeated with the same initial boundary condition at different Rayleigh numbers for each geometrical configuration. The modulus of the velocity vector at different heights (16.1, 26.1 and 36.1 mm from the floor of the enclosure) was subsequently stored after 45 min. As an example, Fig. 5 shows the plot of the modulus of the velocity vector for the three different experiments at $Ra = 2.28 \times 10^5$ in the symmetrical configuration ($d = 0.02$ m) for a height of 26.1 mm. There is clearly a good agreement between these data proving that the repeatability of the test

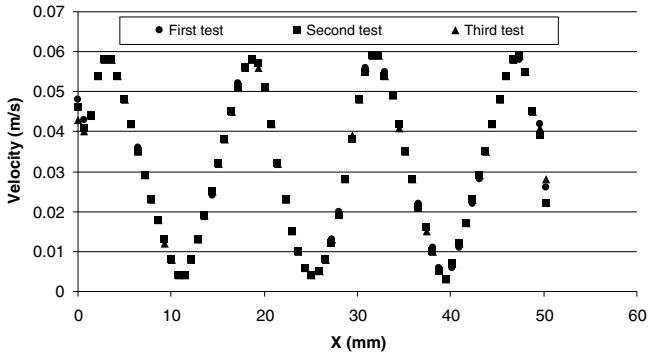

Fig. 5. Plot of the modulus of the velocity vector for a height of 26.1 mm inside the enclosure for three different tests.

was acceptable. The only small difference between the three tests was found near the left side of the cavity. This was due to the reflections of the laser light near the contours of the enclosure which created some noise in the PIV image leading to a lack of precision in the velocity vectors. Similar results were obtained in each test made to determine the repeatability of the experiments.

3.3. Streamlines

Fig. 6 shows the streamlines after 20, 45 and 60 min for $Ra = 2.28 \times 10^5$ and for the three positions analyzed. In these images it is possible to see the creation of two counter-rotating vortexes which depend on the motion of air due to the heating of the strip.

These images also indicate the extreme stationariness of the physical phenomenon in each configuration. In particular it is important to note that, although nebulised oil was sprinkled inside the cavity 20 s before each acquisition step generating a perturbation, the flow regains its stationary configuration.

In Fig. 7 the streamlines can be analyzed for each geometrical configuration at different Rayleigh numbers. The structure of these vortexes does not change with the Rayleigh number only because of the symmetrical position but is also closely connected with the position of the hot strip. In the central configuration, where the hot strip was at a distance $d = 0.02$ m from the right cold vertical wall, it is possible to see the presence of two symmetrical vortexes with the same dimensions (Fig. 7, column a). They did not rotate in the same direction and their rotation axis was parallel to the direction of the length of the cavity (z-axis). Neither their size nor their position inside the cavity were influenced by the variations of the Rayleigh number in this particular configuration unlike the other two positions shown in Fig. 7.

For example, at $d = 0.015$ m it is possible to note that the right cylinder is smaller that the other one. When the velocity map is analyzed, it is clear that they do not have the same strength as in the symmetrical configuration. The vortex in the left side of the enclosure is bigger and stronger than the other one which also has the slowest velocity fields.

Finally, in the last position, where $d = 0.01$ m, the difference between these two convective vortexes is more evident. In fact, on analyzing the image it is possible to see that the location of the strip seems to create a separation between the upper and lower parts of the smaller right vortex particularly at low Rayleigh numbers. The small space that is available for the fluid in the right low side, obstructs good communication between the air in the

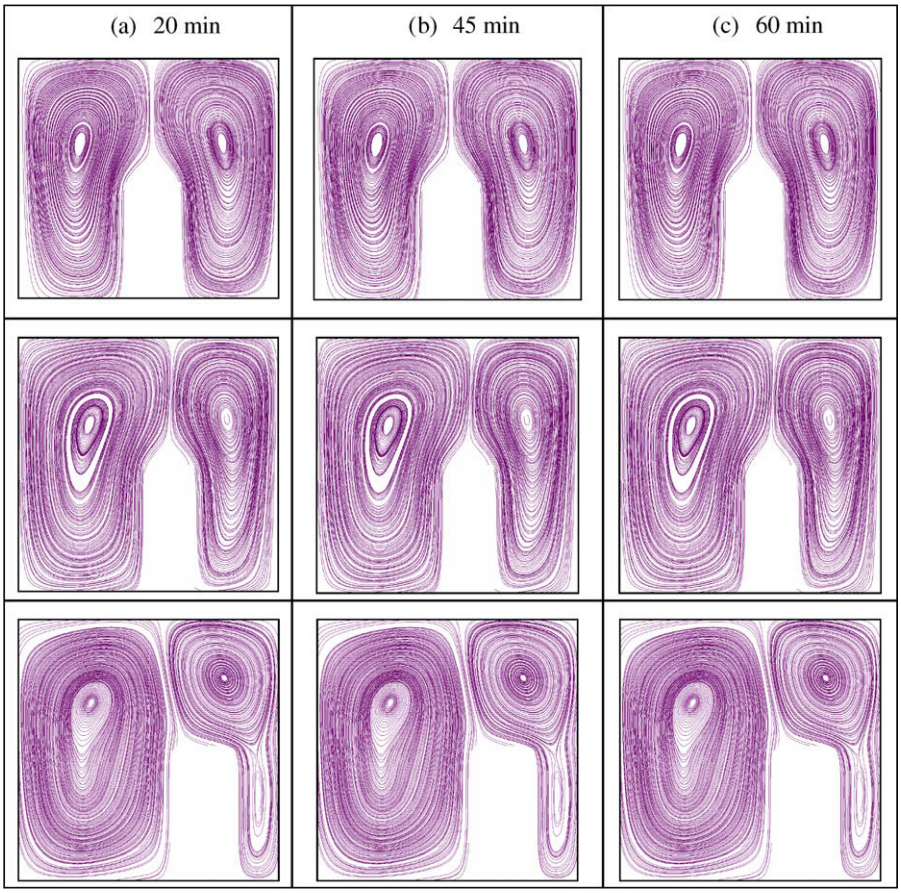

Fig. 6. Streamlines for $Ra = 2.28 \times 10^5$ for $d = 0.02$ m (first row), $d = 0.015$ m (second row) and $d = 0.01$ m (third row).

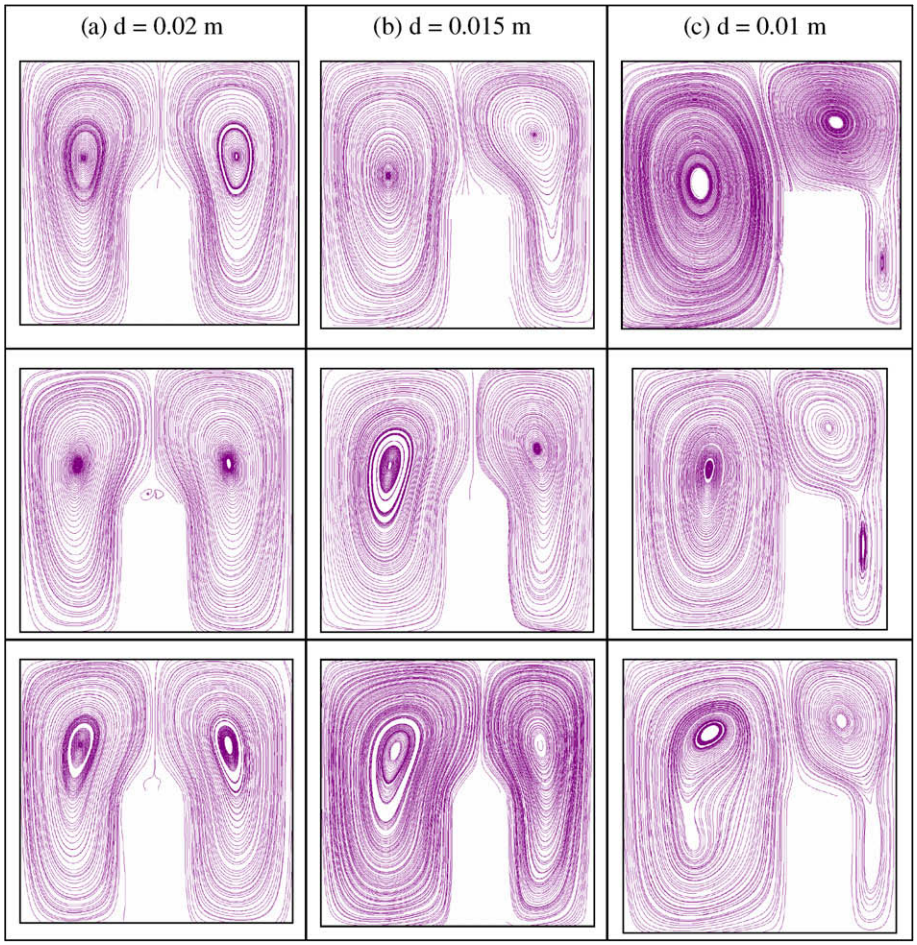

Fig. 7. Streamlines for $Ra = 6.39 \times 10^4$ (first row), for $Ra = 1.78 \times 10^5$ (second row) and for $Ra = 3.16 \times 10^5$ (third row).

superior vortex and the air in the lower part. Therefore, in the latter region the velocity field, as shown below, is very slow. Consequently, the natural convective heat transfer is reduced. Only at the highest Rayleigh numbers it is possible to notice better communication between the two regions of the same vortex as shown in the last frame of Fig. 7, column c.

During this analysis the position of the convective cylinders' line of conjunction was also studied. In particular the analysis focussed on how this position was influenced by the position of the source and by the Rayleigh number. In fact, these factors are important for understanding the relationship between the two large convective cylinders and the two small vertical structures on the upper surfaces.

If the set of images in Fig. 7, column a, is compared with the other positions, it is possible to note that in the first column the contact line of the vortexes is different from the other ones. In fact, in the symmetrical case this line is perpendicular to the hot strip and agrees with the axis of symmetry of the source for each Rayleigh number. Instead, for the asymmetrical configurations the line has a slope that changes with the Rayleigh number. For example, at $d = 0.015$ m for the low Rayleigh numbers, the contact line slopes towards the left vortex (Fig. 7, column b, first row); while by increasing the Rayleigh number the line again becomes almost perpendicular, as shown in the frame in the third row of Fig. 7, column b. At $d = 0.01$ m the differences with the central position are more evident: this line is completely out of the axis of symmetry of the source. Moreover, it slopes towards the left larger vortex for each Rayleigh number analyzed; only at the highest Rayleigh numbers does the slope become less, as shown in the frame of the third row of Fig. 7, column c.

Therefore, it is possible to conclude that the shape and the size of the two convective cylinders in the asymmetrical geometrical configurations, unlike the symmetrical one, are influenced by the Rayleigh number.

3.4. Velocity distribution

Using the 2D-PIV system the distribution of the velocity vectors and the velocity maps were also obtained. The maps shown in this section were obtained after statistical evaluation with the PIV processor. Subsequently, the mean values of the flow fields were produced through a statistical procedure performed on the instantaneous flow fields. The physical phenomenon analyzed showed a very steady and stationary behaviour and for this reason a total of three sets were taken for each Rayleigh number. Each set was made up of 30 pairs of images for a total of 90 images which were used to generate the average flow.

In Fig. 8 it is possible to see the vector velocity distributions for different Rayleigh numbers for each geometrical configuration. These data confirm the symmetrical behaviour of the convective structure for $d = 0.02$ m and the asymmetrical performance for the other geometrical configurations. However, it is also possible to begin to notice the presence of a particular zone near the upper part of the source with very short velocity vectors in particular for $d = 0.02$ m and for $d = 0.015$ m. This characteristic is analyzed thoroughly in the next section although it is already

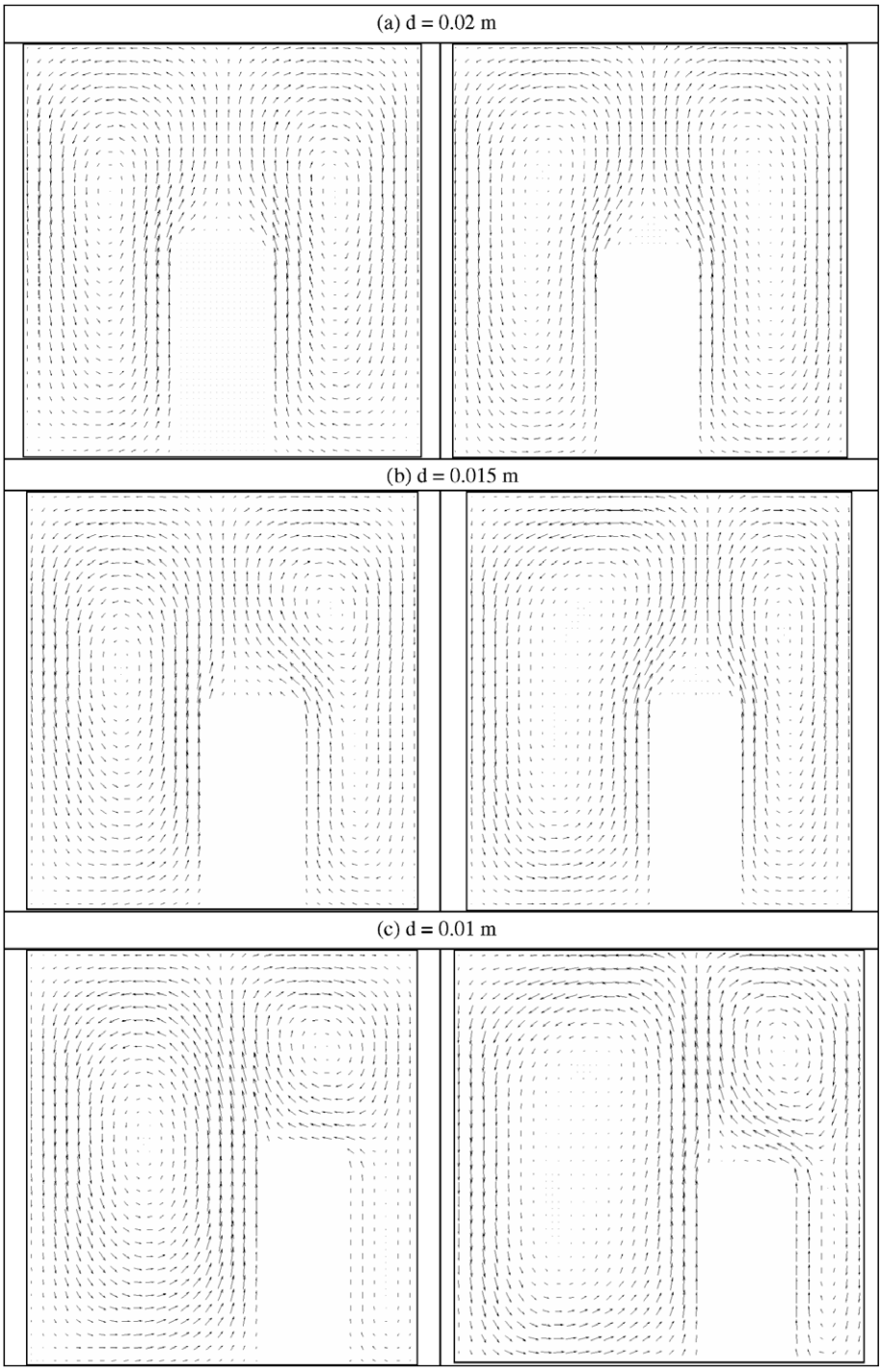

Fig. 8. Velocity vectors for $Ra = 6.39 \times 10^4$ (first column) and for $Ra = 3.16 \times 10^5$ (third column).

possible to see that this region is characterized by a very slow flow indicated by the very short velocity vectors that are similar to small points. In the case of $d = 0.02$ m and $d = 0.015$ m, this zone is always present in each Rayleigh number analyzed; some changes are present at $d = 0.01$ m. The zone is generated by the shape of the source: the upper corners of the source create a separation of the flow that cannot follow the edge of the source as happens along the vertical walls. Some particles of air remain confined in this zone, creating particular structures as shown in detail in the next section.

Finally, Figs. 9–17 show the velocity maps for some Rayleigh numbers in different geometrical configurations. It is possible to note that the modulus of the velocity vectors is closely connected with the Rayleigh number and the geometrical configuration. The velocity field becomes faster with the increase in the Rayleigh number. This is very important for natural convective heat transfer because if the flow is faster, natural convection is more efficient. This growth in the velocity field was seen both for the highest and the average velocity values in each geometrical configuration analyzed.

It is also possible to see how the bigger vortex in each geometrical asymmetrical position obtained the velocity peak at each Rayleigh number analyzed. Moreover, these images confirm that the flow on the upper surface of the source is very slow.

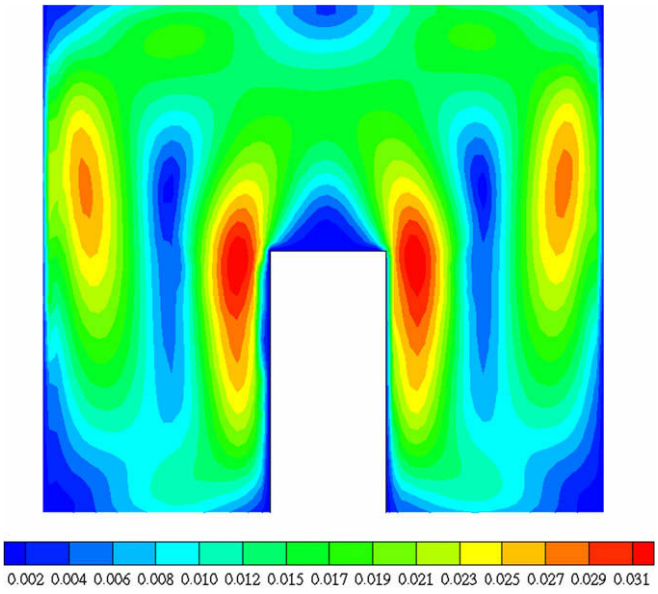

Fig. 9. Velocity map (m/s) for $d = 0.02$ m at $Ra = 6.39 \times 10^4$.

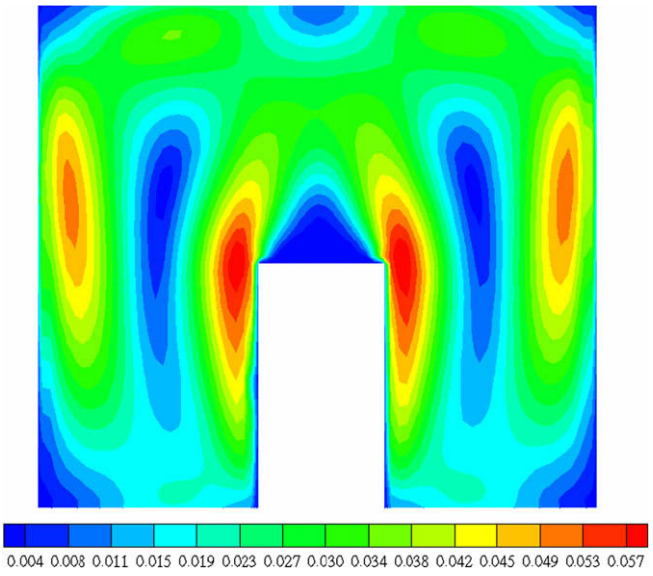

Fig. 10. Velocity map (m/s) for $d = 0.02$ m at $Ra = 1.78 \times 10^5$.

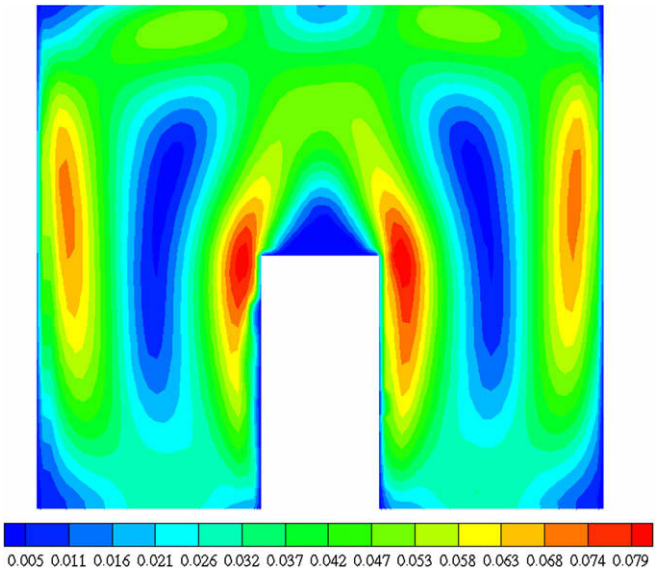

Fig. 11. Velocity map (m/s) for $d = 0.02$ m at $Ra = 3.16 \times 10^5$.

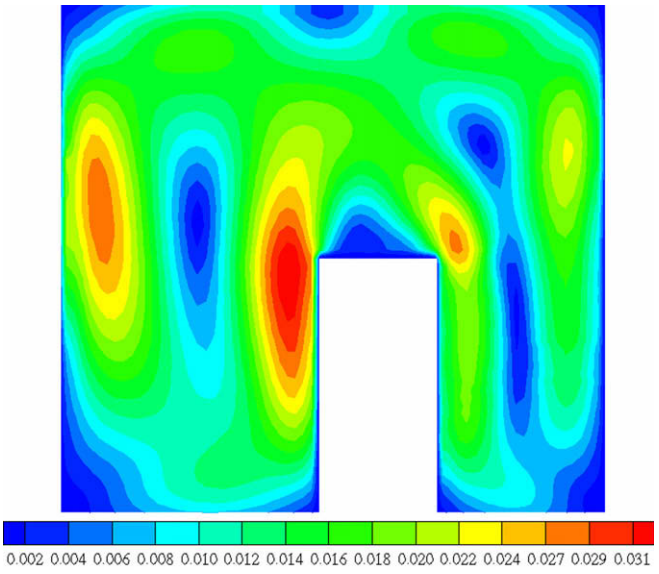

Fig. 12. Velocity map (m/s) for $d = 0.015$ m at $Ra = 6.39 \times 10^4$.

Finally, it is also clear that the geometrical configuration influences the modulus of the velocity vectors. Table 5 shows the peak and average velocity values for the three positions analyzed and for each Rayleigh number.

Particularly in the symmetrical configuration, where $d = 0.02$ m, for the same Rayleigh number, the highest velocity values were nearly always captured both for the velocity peak and for the average velocity values with respect to the other configurations. This behaviour is more evident at high Rayleigh numbers although even at low numbers some differences can be seen. In Table 6 it is also possible to see this difference from a quantitative point of view. The values shown in this table were obtained by calculating the difference between the peak velocity and the average velocity value, stored in the symmetrical configuration and used as the reference position, and the corresponding value of the two other configurations at the same Rayleigh number. Analyzing these data it is possible to note that the central configuration (Figs. 9–11) almost always has the highest velocity field both for the peak velocity value and for the average one., Relevant percentage differences were not found only at the lowest Rayleigh numbers but under these conditions the flow was not very fast and it was therefore more difficult to notice considerable differences.

However, thanks to these results it is possible to assert that the symmetrical geometrical configuration, where d is 0.02 m, showed the highest velocity field for each Rayleigh number analyzed. For this reason it may be hypothesised that a faster velocity flow for this configuration ensures a better natural convection heat transfer. For $d = 0.02$ m it is possible to obtain the best position of the hot strip in order to create the fastest velocity field able to remove the heat generated inside the cavity in the best way.

3.5. The small vortexes

Analyzing the dynamic behaviour of the natural convection in the test cell, it is possible to note the presence of two small vortical

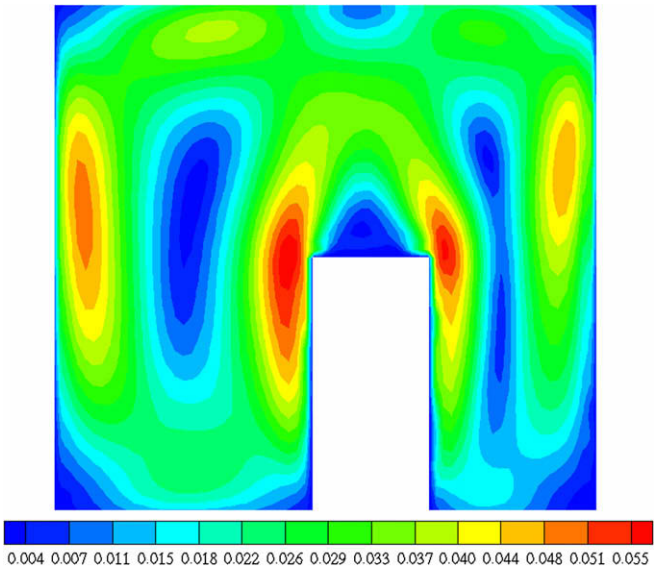

Fig. 13. Velocity map (m/s) for $d = 0.015$ m at $Ra = 1.78 \times 10^5$.

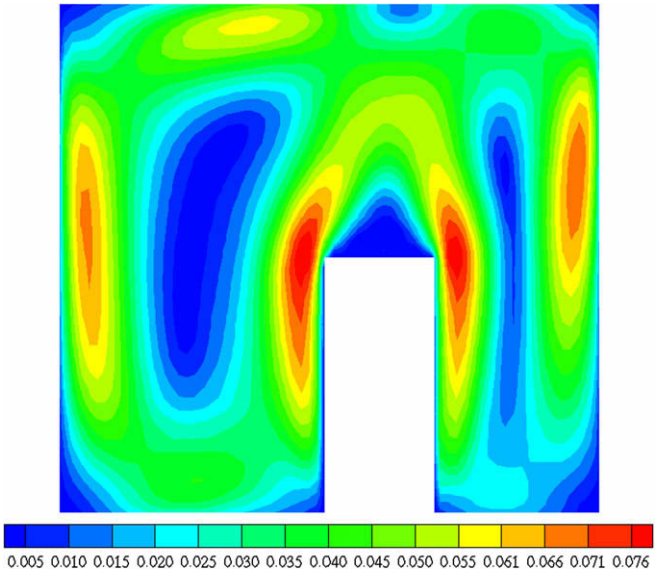

Fig. 14. Velocity map (m/s) for $d = 0.015$ m at $Ra = 3.16 \times 10^5$.

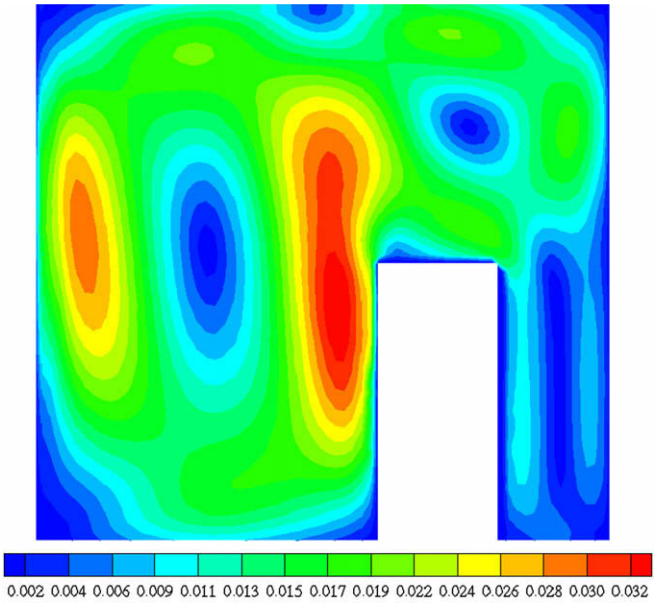

Fig. 15. Velocity map (m/s) for $d = 0.01$ m at $Ra = 6.39 \times 10^4$.

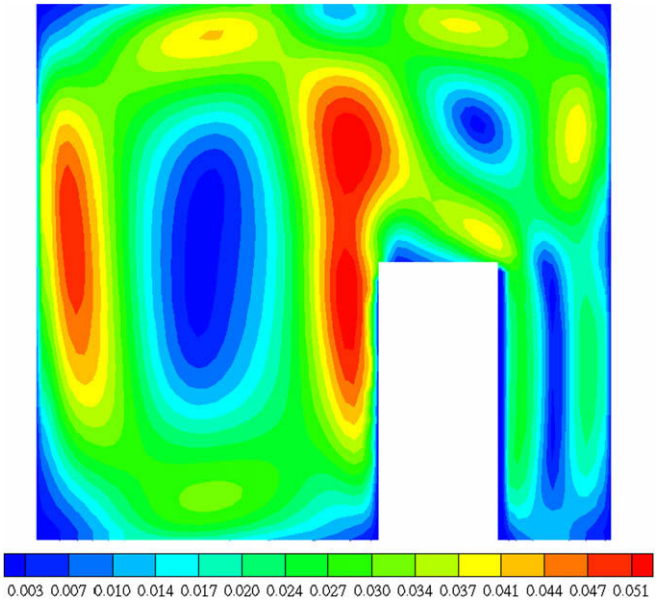

Fig. 16. Velocity map (m/s) for $d = 0.01$ m at $Ra = 1.78 \times 10^5$.

structures located on the upper surface of the hot strip, as shown in Fig. 18. A specific analysis was carried out in order to study these structures in more detail. On the basis of the previous results it was supposed that the flow near this surface was very slow. Therefore, the Δt between the two laser flashes was modified so as to capture images that were able to identify these structures. The tests were carried out with Δt values of about 60,000 μs.

Fig. 19 shows that these small vortexes are not present at each Rayleigh number and for each geometrical configuration. At low Rayleigh numbers there are no vortical structures. For example, for $Ra = 6.39 \times 10^4$ (Fig. 19 column a), the flow has an ascending motion without the creation of any vortexes either for $d = 0.02$ m or for $d = 0.015$ m. However, if the Rayleigh number increases, as shown in Fig. 19, column b, these two small vortexes are evident. They are generated by the air that remains confined inside the small zone (described in the previous section) on the upper surface of the hot strip. This zone is created by the two large vortexes. The particles of air that glide on the lateral vertical hot surfaces break off from the corner of the strip. This behaviour generates a stagnation zone where there are some air particles that create this particular motion depending on the Rayleigh number and on the position of the source. The vortexes, shown in Fig. 19, column b, are counter-rotating and are in contact with the large vortexes along the line that identifies the separation of the flow from the source profile, as shown in Fig. 18, column b.

With low Rayleigh numbers the heat rate generated by the upper surface of the source cannot generate the vortexes. In this condition, the flow rises towards the top of the cavity and when it reaches the two large cylinders is sucked into them. On the contrary, with higher Rayleigh numbers the vortexes develop. They rotate in the opposite direction to their respective large vortexes and tend to maintain their own independence. The line, along which they enter in contact with the large vortexes, becomes an isolation zone that makes them two independent structures.

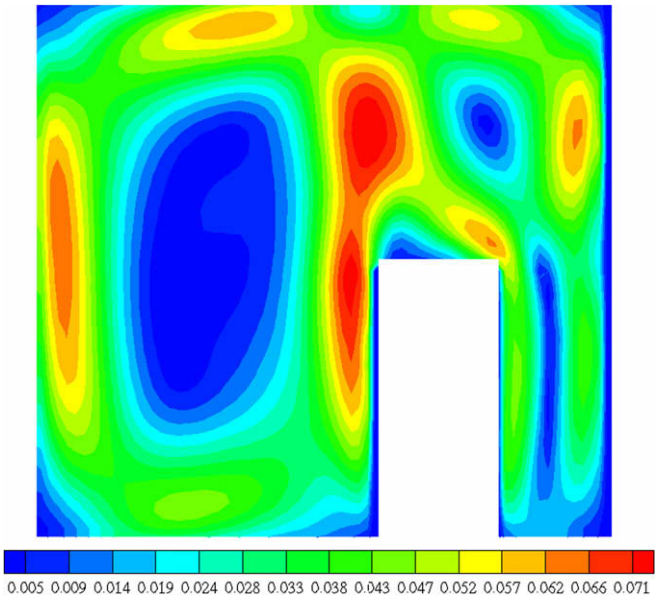

Fig. 17. Velocity map (m/s) for $d = 0.01$ m at $Ra = 3.16 \times 10^5$.

Table 5
Peak and average velocity values for each Rayleigh number and in each geometrical position

Ra	$d = 0.02$ m		$d = 0.015$ m		$d = 0.01$ m	
	V_{peak} (m/s)	$V_{average}$ (m/s)	V_{peak} (m/s)	$V_{average}$ (m/s)	V_{peak} (m/s)	$V_{average}$ (m/s)
6.39×10^4	0.033	0.01443	0.033	0.01387	0.032	0.01417
1.21×10^5	0.048	0.01999	0.047	0.01998	0.044	0.01999
1.78×10^5	0.061	0.02593	0.059	0.02496	0.054	0.02488
2.28×10^5	0.07	0.03013	0.068	0.02862	0.061	0.02738
2.73×10^5	0.077	0.03367	0.077	0.03228	0.069	0.03021
3.16×10^5	0.084	0.03636	0.081	0.03372	0.076	0.03244

Table 6
Comparison between the maximum and average velocity values for the symmetrical configuration compared with the same values for the other positions

Ra	$d = 0.015$ m		$d = 0.01$ m	
	$\Delta_{peak\ value}$ (%)	$\Delta_{average\ value}$ (%)	$\Delta_{peak\ value}$ (%)	$\Delta_{average\ value}$ (%)
6.39×10^4	0	4	3	1.8
1.21×10^5	2	0.6	8.3	0
1.78×10^5	3.3	3.7	11.5	4
2.28×10^5	2.8	5	12.8	9.1
2.73×10^5	0	4.1	10.4	10.3
3.16×10^5	3.6	7.2	9.5	10.8

It is possible to find these two small vortexes only for Rayleigh numbers up to $Ra = 9 \times 10^4$ and for the position with $d = 0.02$ m and $d = 0.015$ m. When the hot strip is fixed at $d = 0.01$ m the structure of the right main vortex succeeds in keeping the flow attached to the profile of the source and consequently the stagnation zone is absent. If the image in Fig. 8, column c, is checked, it is possible to see how the velocity vectors for $d = 0.01$ m stay attached to the upper surface of the cavity. Only at $Ra = 3.16 \times 10^5$ (the image in the third row of column c in Fig. 8) does a small separation appear near the right side of the source but it is not enough to create any structures.

This characteristic is of a certain importance in the heat transfer. For $d = 0.01$ m the flow on the upper surface of the strip proves to be faster than the other two configurations. Therefore, in this case, a more efficient local movement of the air was found which succeeded in removing more heat from this zone thanks to a higher velocity field.

4. Conclusions

In this paper, the influence on natural convection of the position of a hot strip inside a square cavity was analyzed. A cell with a side $H = 0.05$ m was used in the test. The source had a thickness $l = 0.01$ m, height 0.025 m and the same length as the enclosure, $L = 0.42$ m. It was greater than H in order to ensure that it is long enough to limit the air motion developed along the z-axis to such an extent that it becomes negligible. Consequently, it was possible to neglect the end effect and to consider the problem as a two-dimensional one.

Three different positions were analyzed at the steady state and under laminar conditions. The first position was a symmetrical configuration with a distance between the right surface of the strip and the right cold side of the enclosure of $d = 0.02$ m. In the other two configurations this parameter was changed, using $d = 0.015$ m and $d = 0.01$ m.

The study was carried out with an experimental set-up using a non-intrusive technique to evaluate the dynamic structures and the dynamic quantities indispensable for describing the physical phenomenon.

A 2D-PIV system was used in order to obtain the streamlines, the velocity vector distributions and the velocity maps at different Rayleigh numbers.

The Rayleigh numbers analyzed ranged from 6.5×10^4 to 3.2×10^5. The quality of the experimental data was evaluated in each test in particular to assess their repeatability and the stationary state of the physical phenomenon.

During the tests it was observed that, when the strip started to become warm, a movement of air developed inside the enclosure creating two anti-clockwise cylinders. These two vortexes were closely connected with the geometrical configuration. In the symmetrical position the shape of the vortexes was independent from the Rayleigh number analyzed. Their line of contact remained perpendicular to the hot strip in each test. On the contrary, in the other two configurations, the left vortex became larger than the right one. As described above, their line of contact sloped in the direction of the large vortex.

These differences in the main dynamic structures, connected with the position of the source, influenced the whole velocity field. In particular, on analyzing the velocity maps, it is possible to note that the velocity fields of the symmetrical configuration are faster than the ones recorded for $d = 0.015$ m and $d = 0.01$ m with the same Rayleigh number. If the flow is faster inside the cavity when the strip is put in the middle, it can remove more heat from the source and therefore the convective heat transfer is better in the symmetrical configuration than in the asymmetrical ones.

Finally, the presence of small vortical structures on the upper surface of the hot strip were also observed. They required a dedicated study because their velocity field is very slow. Thanks to this analysis it was possible to see that the vortexes were generated by flow separation in proximity to the corners of the strip. They were present only for $d = 0.02$ m and for $d = 0.015$ m for Rayleigh numbers up to 9×10^4 and they remained independent from the large cylinders.

The presence of these two small vortexes generated a small zone, on the upper surface of the hot strip for $d = 0.02$ m and $d = 0.015$ m, where a very slow velocity field was captured. Consequently, it is possible to conclude that if the air particles are almost still in this zone, they do not ensure such a good natural heat transfer on the upper side of the strip as occurs on the lateral walls. However, since this effect is localized on the smallest side of the

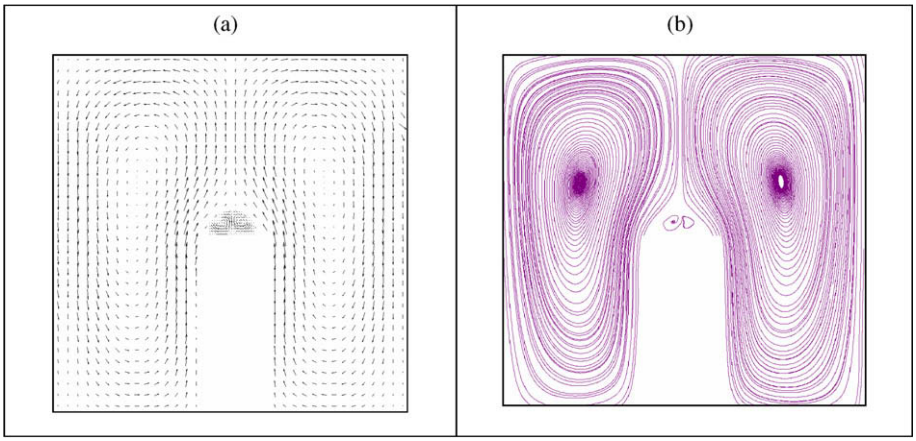

Fig. 18. Position of the small vortical structures for 1.78×10^5.

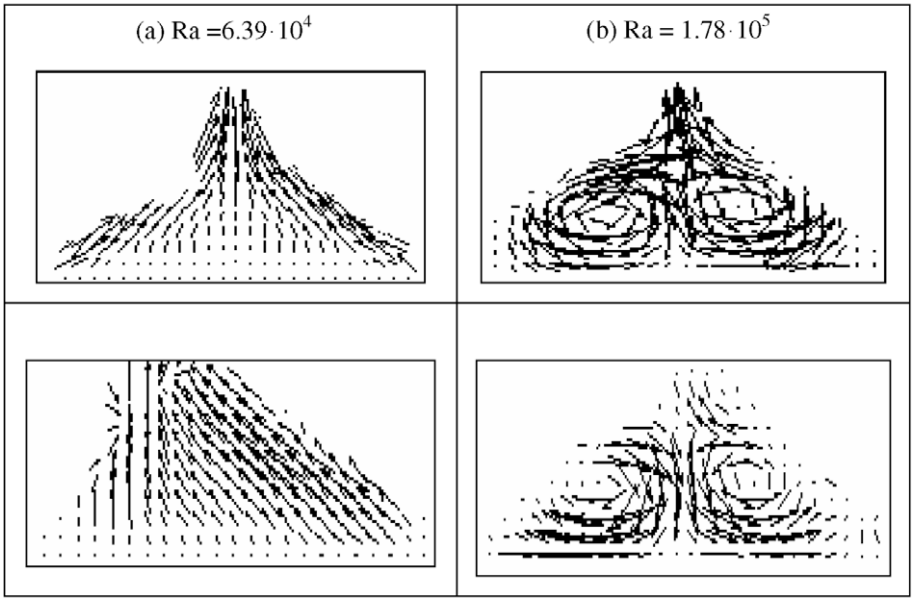

Fig. 19. Detail of the vortical structures on the upper surface of the strip for $d = 0.02$ m (first row) and for $d = 0.015$ m (second row).

source the symmetrical configuration is still the one which on the whole ensures the fastest velocity field and therefore creates the best dynamic conditions for developing good natural convection.

References

[1] G. Cesini, M. Paroncini, G. Cortella, M. Manzan, Natural convection from a horizontal cylinder in a rectangular cavity, Int. J. Heat Mass Transfer 42 (1999) 1801–1811.
[2] R.A.V. Ramos, L.F. Milanez, Numerical and experimental analysis of natural convection in cavity heated from below, in: Proceedings of the 11th IHTC Kyongju, Korea, vol. 3, 1998.
[3] A. Valencia, R.L. Frederick, Heat transfer in square cavities with partially active vertical walls, Int. J. Heat Mass Trans 32 (1989) 1567–1574.
[4] O. Aydin, W.J. Yang, Natural convection in enclosures with localized heating from below and symmetrical cooling from sides, Int. J. Num. Meth. Heat Fluid Flow 10 (2000) 519–529.
[5] E. Ntibarufata, M. Hasnaoui, E. Bilgen, P. Vasseur, Natural convection in partitioned enclosures with localized heating, Int. J. Num. Meth. Heat Fluid 3 (1993) 133–143.
[6] H. Oztop, E. Bilgen, Natural convection in differentially heated and partially divided square cavity with internal heat generation, Int. J. Heat Fluid Flow 48 (2005) 1470–1479.
[7] M.T. Stickland, T.J. Scanlon, J. MacKenzie, An experimental investigation of natural convection with solidification in a differentially heated cavity, Int. J. Heat Mass Transfer 5 (2007) 36–44.
[8] S. Acharya, R. Jetli, Heat transfer due to buoyancy in a partially divided square box, Int. J. Heat Mass Transfer 33 (1990) 931–942.
[9] R. Anderson, A. Bejan, Heat transfer through single and double vertical walls in natural convection: theory and experiment, Int. J. Heat Mass Transfer 24 (1981) 1611–1620.
[10] M. Raffel, C. Willert, J. Konipenhans, Particle Image Velocimetry, Springer, Heidelberg, Berlin, 1998, ISBN 3-540-63683-8.
[11] Dynamic Studio software and Introduction to PIV Instrumentation, Dantec Dynamics GmbH, 2000, Publication number: 9040U3625.